International Journal of Biological Macromolecules 381 (2026) 154286

Contents lists available at ScienceDirect

International Journal of Biological Macromolecules

journal homepage: www.elsevier.com/locate/ijbiomac

# Short-life bamboo lignocellulose is superior-convertible for advanced bioethanol and nanomaterials to decline $CO_2$ emission and environmental impacts

Hairong Gao [a,b,c,1], Boyang He [a,c,1], Yixiang Wang [a,c,1], Hao Peng [a], Peng Liu [a], Yongtai Wang [a,c], Yanting Wang [a], Qiang Li [d], Zhi Qi [e], Hua Yu [a], Xinchun Lin [b,*], Liangcai Peng [a,c,**,2]

[a] Key Laboratory of Fermentation Engineering (Ministry of Education), Hubei Key Laboratory of Industrial Microbiology, Biomass & Bioenergy Research Center, School of Life & Health Sciences, Hubei University of Technology, Wuhan, 430068, China
[b] State Key Laboratory of Subtropical Silviculture, Zhejiang A & F University, Lin'an, 311300, China
[c] College of Plant Science & Technology, Huazhong Agricultural University, Wuhan, 430070, China
[d] College of Engineering, College of Horticulture & Forestry Sciences, Huazhong Agricultural University, Wuhan, 430070, China
[e] State Key Laboratory of Herbage & Endemic Crop Biotechnology, School of Life Sciences, Inner Mongolia University, Hohhot, 010070, China

ARTICLE INFO

*Keywords:*
Bamboo
Bioethanol
Nanomaterials
Environmental impacts
Life cycle assessment

ABSTRACT

Efficient utilization of bamboo lignocellulose remains challenging because its recalcitrance limits biomass conversion and utilization. Here, we demonstrate a cascading biorefinery strategy of one-year-old (Y1) bamboo by maximizing bioethanol production and converting all enzymatic residues into high-value nanomaterials. While the global lignocellulose harvest of Y1 bamboo was estimated for boosting sugars and bioethanol production, the enzyme-undigested residues were recycled to generate smaller cellulose nanofibrils and shorter cellulose nanocrystals by 21% and 50%, compared to its raw material and other 3- and 5-year-olds bamboo samples. The ultrafine lignin nanoparticles of Y1 undigested-residues with 92%–96% reduced diameters were subsequently obtained to generate the graphitic nanocarbon with the second largest specific-surface-area at 2865 $m^2\ g^{-1}$ among the most biomass-based carbons as previously reported. The nanocarbon was detected with much higher specific electro-capacitance at 261 F $g^{-1}$ and consistently higher $CO_2$ adsorption capacity at 4.3 mmol $g^{-1}$. Notably, the 75-year life cycle assessments anticipate total carbon captures from advanced bioethanol and nanomaterials productivity of the Y1 bamboo, which may decline global warming and environmental impacts by replacing petrol-fuels and low-value bioproducts. This study thus demonstrates that short-life bamboo offers multiple recycling advantages for efficient biofuel conversion and effective bioproduct invention associated with the integrative reduction of total $CO_2$ emissions by cascading lignocellulose utilization and zero-biomass liberation.

## 1. Introduction

Carbon neutrality is considered a long-term strategy for controlling global warming and climate abnormity [1,2]. As plant photosynthesis provides a sustainable $CO_2$ fixation path to accumulate countless biomass in plant cell walls, lignocellulose conversion can partially replace fossil fuels and reduce net carbon emissions. However, lignocellulose recalcitrance inevitably results in expensive biomass dispensation objectionable for large-scale biofuel production, along with secondary waste liberation [3–6]. Thus, the integration of various green-like technologies is crucial to generating cost-effective biofuels and value-added nanomaterials with sustainable circulation [7–9].

* Corresponding author.
** Correspondence to: L. Peng, Key Laboratory of Fermentation Engineering (Ministry of Education), Hubei Key Laboratory of Industrial Microbiology, Biomass & Bioenergy Research Center, School of Life & Health Sciences, Hubei University of Technology, Wuhan, 430068, China.
*E-mail addresses:* lxc@zafu.edu.cn (X. Lin), lpeng@mail.hzau.edu.cn (L. Peng).
[1] The authors contribute equally.
[2] Web: http://bbrc.hbut.edu.cn.

https://doi.org/10.1016/j.ijbiomac.2026.154286
Received 4 April 2026; Received in revised form 20 August 2026; Accepted 29 August 2026
Available online 1 September 2026

Given that cellulosic ethanol is an excellent additive for gasoline, lignocellulose conversion retains many enzyme-undigested residues rich in condensed lignin with highly crystalline cellulose [10–12]. As a promising solution, lignin is widely employed to generate valuable bioproducts, with lignin nanoparticles (LNPs) anticipated to be active precursors for high-quality nanomaterials [13,14]. As essential load-bearing wall compounds in higher plants, cellulose microfibrils are progressively retained to fabricate dimension-reduced cellulose nanofibrils (CNFs) and cellulose nanocrystals (CNCs) as functional compositors and optimal intermediates for the generation of ultrafine nanocarbons [15–18]. Nanocarbon materials are currently available in a range of dimensionalities from zero-dimensional (0D) quantum dots to three-dimensional (3D) bulk materials, and exhibit favorable stability and other advantageous properties [19–22]. Owing to their large specific surface areas, adjustable pore sizes, and superior physicochemical stabilities, the carbonaceous materials have attracted significant attention as electrode materials for supercapacitors [23,24]. Despite these advantages, the widespread application of nanocarbon-based supercapacitors is hindered by their relatively low energy densities and high manufacturing costs. The transforming of amorphous carbon into graphitic carbon can improve the catalytic performance of transition metals and carbon materials [25–27].

As a typically perennial plant, bamboo has an extremely rapid growth rate, with woody stems that can grow up to 1 m per day [28], and provides a vast supply of lignocellulosic materials worldwide [28,29]. Although advanced technology has been developed to utilize mature bamboo for biofuels and bioproducts, many unconvertible biomass residues remain preserved owing to the exceptionally harsh recalcitrance of bamboo lignocellulose with compacted lignification and high crystallinity. By performing green-like pretreatments for three different-year-old bamboo tissues distinct from lignocellulose recalcitrance, our previous study examined enhanced biomass enzymatic saccharification and bioethanol production from one-year-old bamboo. However, whether short-life bamboo offers superior cascading potential for simultaneous biofuel generation and advanced nanomaterial fabrication has not yet been systematically evaluated. Furthermore, the long-term carbon mitigation potential of such an integrative strategy remains unclear. In the current study, the total global bioethanol production from green-like bamboo processes was evaluated, and all the remaining enzyme-undigested residues were subsequently utilized to generate superfine CNFs, CNCs, and LNPs (Fig. 1). In addition, the enzyme-undigested residues were converted into graphitic nanocarbon through optimized thermo-chemical catalysis to obtain high electrochemical capacitance and $CO_2$ adsorption capacity. Finally, this study conducts a predictable life-cycle assessment (LCA) of bioethanol and advanced nanomaterials productions from one-year-old bamboo harvested and estimates the alternative advantages of traditional fossil fuels and low-priced bioproducts for sustainably reducing $CO_2$ emissions and environmental impacts.

## 2. Material and methods

### 2.1. Materials

Bamboo (*Phyllostachys edulis*) was grown in the experimental field of Zhejiang A&F University. The 1-, 3- and 5-year-old bamboo stems,

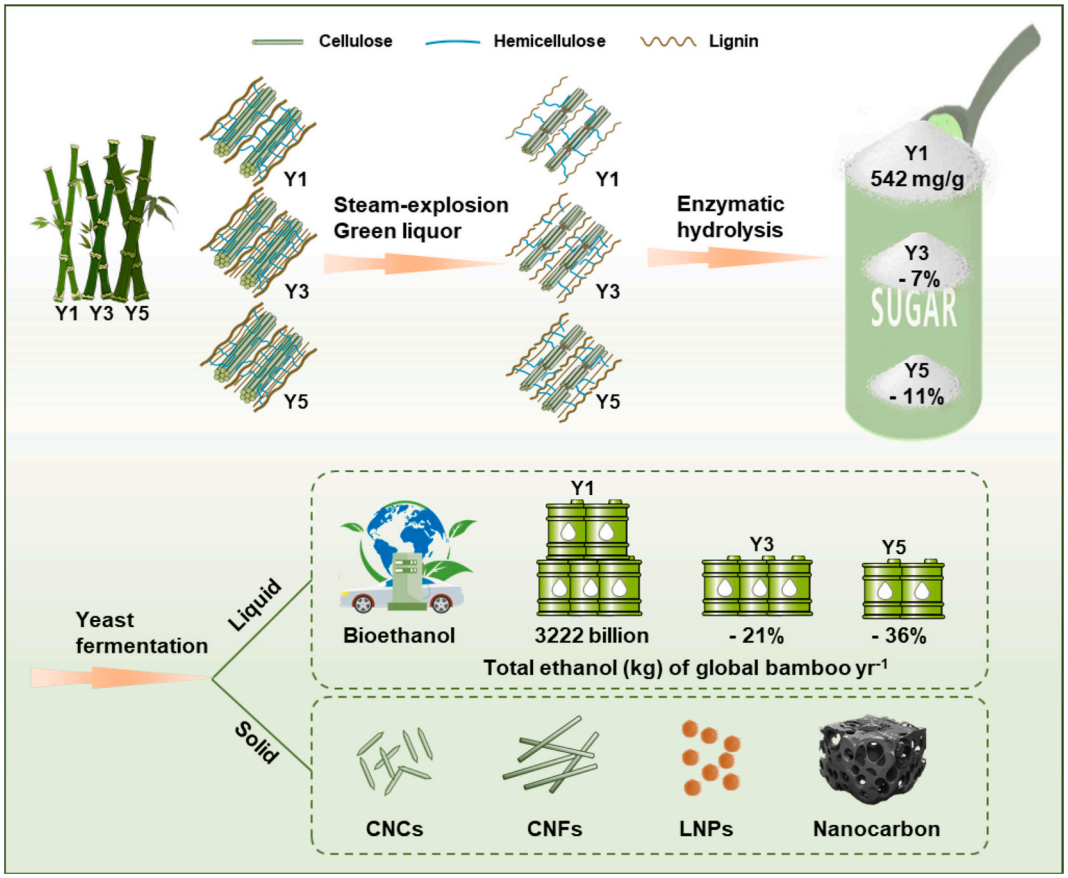


**Fig. 1.** General estimation of global bioethanol production and advanced nanomaterials conversion from different-year-old bamboo harvests. The 1-, 3-, and 5-year-old bamboo samples termed as Y1, Y3, and Y5; after two-step (steam explosion followed with green liquor) pretreatments and sequential enzymatic hydrolyses, total sugars yield of Y1 bamboo was estimated to account for bioethanol production, and total global bioethanol yields were calculated based on world-wide bamboo harvests for 75 years as described in Table S1; the sugars and bioethanol yields of Y3 and Y5 bamboo samples were presented as reduced percentage relative to the Y1 bamboo; the enzyme-undigested residues were employed to generate four types of nanomaterials.

termed PhY1/Y1, PhY3/Y3, and PhY5/Y5, were respectively collected, and two-step pretreated lignocelluloses of bamboo samples were collected as previously described [30]. Briefly, the air-dried bamboo chips (0.3 × 0.3 × 5 cm) were pretreated by steam explosion at 213 °C (2.5 MPa) for 5 min. The resulting residues were then subjected to green liquor (a mixture of $Na_2S$ and $Na_2CO_3$, sulfidity 30%) pretreatment under optimized conditions (TTA = 31.0%, 166.41 °C, 28.01 min). After pretreatment, the residues were thoroughly washed with deionized water until neutral pH. The pretreatment supernatants were collected for lignin isolation as described [31], and solid enzyme-undigested residues were stored as undigested residues as described (Fig. S1). Briefly, the pretreatment supernatant was neutralized and concentrated, followed by ethanol-induced precipitation to recover hemicelluloses. The remaining liquor was acidified to pH 2 to precipitate lignin, which was collected by centrifugation, washed to remove salts, and freeze-dried for further analysis. After fermentation, the remaining solid fraction was recovered by filtration, thoroughly washed with deionized water to remove sugars and enzymes, and freeze-dried as the enzyme-undigested residue (Fig. S1). This residue was subsequently used for preparations of CNFs, CNCs, LNPs, and nanocarbon.

### 2.2. CNFs and CNCs preparation

The major steps for CNFs and CNCs preparations were listed (Fig. S1). Briefly, dried and milled bamboo samples were delignified with 5% NaOH at 60 °C for 1 h (5 cycles) and bleached with 0.5% NaClO at 60 °C for 1 h (3 cycles). The solids were washed to neutral pH and homogenized (60 MPa, 5–20 cycles) to obtain CNFs [32]. For CNCs, the purified cellulose (2 g) was hydrolyzed with 64% $H_2SO_4$ at 45 °C for 45 min, followed by centrifugation and dialysis to neutral pH. The suspension was ultrasonicated for uniform dispersion and stored at 4 °C for further use [17,18].

### 2.3. LNPs fabrication

LNPs were obtained by solvent-antisolvent method [33] with minor modification (Fig. S1). Lignin powders (0.3 g) were mixed with 6 mL glycerol-water solution (9:1, v/v) containing 1% HCl into a round bottom flask with stirring at room temperature. The mixture was transferred to a microwave reactor (WBF Y-201, Kebei, China) under irradiation at 400 W for 5 min. After centrifugation at 14000 r/min for 15 min, the supernatant containing LNPs was collected under sonication for 120 min. Under dialysis (MWCO: 8,000–14,000, Spectrum Labs, USA) for 3 days, the LNPs suspension was stored at 4 °C until in use.

### 2.4. Porous nanocarbon preparation

Porous nanocarbon was prepared by pyrolysis followed by $K_2FeO_4$-assisted activation with the enzyme-undigested residues as previously described (Fig. S1). Lignocellulose samples were pyrolyzed in a tube furnace at 400 °C for 2 h at a heating rate of 5 °C $min^{-1}$ under nitrogen as described (Fig. S1). The dispersed $K_2FeO_4$ (99.99%, Aladdin) was added into the pyrolytic carbon (1.0 g) under stirring for 8 h, and dried at 80 °C overnight. The mass ratio of pyrolytic carbon to activator ($K_2FeO_4$) was set at 1:1, 1:2, and 1:3 (w/w) to investigate the effect of activation intensity on pore development and structural evolution. The obtained solid sample was ground into a tube furnace and heated at 700 °C, 800 °C, 900 °C, and 1000 °C for 2 h at a heating rate of 5 °C $min^{-1}$ under argon. After washing with 1 M HCl and deionized water and drying at 100 °C, the carbon sample was stored in use.

### 2.5. Wall polymers extraction and determination

Wall polysaccharides were extracted as previously described and determined as described [34,35]. Using potassium phosphate buffer (pH 7.0), chloroform-methanol (1:1, v/v), DMSO-water (9:1, v/v), and ammonium oxalate 0.5% (w/v), the lignocellulosic biomass was sequentially extracted to remove soluble sugars, lipid, starch, and pectin. The remaining residues were further extracted with 4 M KOH (with 1.0 mg $mL^{-1}$ sodium borohydride) at 25 °C for 1 h, and the supernatants were defined as the KOH-extractable hemicellulose fraction. The remaining residue was used to detect the total pentoses for the non-KOH extractable hemicellulose fraction. The total hemicellulose content was measured by counting the pentoses of the non-KOH-extractable residue and the total hexoses and pentoses in the KOH-extractable supernatant. Total lignin was measured using the Laboratory Analytical Procedure of the National Renewable Energy Laboratory as described [36]. The acid-insoluble and acid-soluble lignin were respectively determined after two-step sulfuric acid hydrolysis, and total lignin was calculated as the sum of both fractions. The lignin monomer composition (H, G, and S units) was determined by alkaline nitrobenzene oxidation followed by HPLC analysis as previously described with minor modifications [37]. The extractive-free cell wall residue was oxidized in alkaline nitrobenzene at 170 °C for 3.5 h, and the resulting oxidation products were analyzed using a Waters 1525 HPLC equipped with a C18 column and UV detection at 280 nm. The degree of polymerization (DP) and crystalline index (CrI) of cellulose samples were respectively detected as described [38]. The crude cellulose samples were prepared for DP detection using 4 M KOH containing sodium borohydride at 1.0 mg $mL^{-1}$ and 8% (w/v) $NaClO_2$, and the DP measurements were completed at 25 ± 0.5 °C under independent triplicate. The X-ray diffraction method was applied to detect cellulose CrI using a Rigaku D/MAX instrument (Ultima III, Japan) according to the equation: $CrI = 100 \times (I_{200}–I_{am})/I_{200}$. $I_{200}$ is the intensity of the 200 peak ($I_{200}$, $\theta$ = 22.5°).

### 2.6. Characterization of nanomaterials

Atomic force microscopy (AFM, SPM9700, China) was employed to observe the CNFs and CNCs samples as described [32,39]. Samples were deposited onto freshly cleaved mica substrates, air-dried, and imaged under tapping mode at room temperature. The average distance between two defects/amorphous chains of cellulose microfibrils was measured using the Gwyddion software. Transmission electron microscopy was applied to observe CNFs, CNCs, and LNPs as described [40,41]. Carbon samples were characterized using the following facilities such as scanning electron microscope (SEM; JSM-6390/LV, Hitachi, Tokyo, Japan), X-ray diffraction spectrometer (XRD, Rigaku-D/MAX instrument, Ultima III, Japan) with Cu Kα radiation; laser scanning confocal micro-Raman spectrometer (IN VIA, Renishaw, UK) with a laser excitation wavelength of 532 nm and scanning in an extended range of 500–3000 $cm^{-1}$. The specific surface area and pore volumes were measured using nitrogen adsorption-desorption (Micromeritics ASAP 2020, US) at 77 K, and the samples were outgassed under vacuum at 200 °C for 2 h before analysis. Under Brunauer–Emmett–Teller (BET) assay, the surface area was determined from the linear plots, and the pore size distribution was calculated.

### 2.7. Electrochemical characterization

The electrochemical properties of carbon samples were evaluated in a three-electrode system with 1 M $Na_2SO_4$ or 6 M KOH as described [42,43]. Carbon powder was loaded on the electrode at ~4.0 or ~10.0 mg $cm^{-2}$. Platinum foil was used as the counter electrodes, and Ag/AgCl and saturated calomel electrode was applied as the reference electrode [42]. The cyclic voltammetry (CV) and galvanostatic charge-discharge (GCD) measurements were completed on a CHI-660E electrochemical workstation (CH Instruments Inc., Shanghai). Based on the GCD curves, the specific capacitance of carbon powder (*Cs*, F $g^{-1}$) was calculated by the equation [44]:

$$Cs = (I \times \Delta t)/(m \times \Delta V) \quad (1)$$

where I (A), Δt (s), ΔV (V) and m (g) represent discharge current, discharge time, operating potential and the total mass of carbon powder without super-P and binder, respectively.

### 2.8. Measurement of $CO_2$ adsorption

$CO_2$ adsorption was detected by a Micromeritics Tristar II 3020 instrument fitted with an external water circulator. After degassing under vacuum overnight at 250 °C, the carbon samples were employed to measure adsorption isotherms at 0 °C and 25 °C and a pressure range of 1 bar, as described [45,46].

### 2.9. Life cycle assessment (LCA)

The LCA was employed to assess the environmental impacts of both bioethanol conversion and four types of nanomaterials generation. The "cradle-to-gate" LCA was defined by major stages of bioethanol production, including feedstock grinding, two-step pretreatment, enzymatic scarification, ethanol fermentation and distillation, as well by the major processes of nanomaterials generation as described (Fig. S1). The LCA was modelled using an attributional approach on process inputs and outputs, and calculations were performed using the SimPro software (version 9.5) in accordance with ISO 14040 guidelines. The selected functional unit was the consumption of 1 kg raw material of bamboo for bioethanol conversion and nanomaterials generation. In particular, the CML 2001 method was employed in this study. Data related to the environmental impact of materials and energy input were mainly obtained from the ecoinvent 3 database using cut-off system model. In this study, we assumed that an equal distribution of enzyme-undigested residues could be allocated to prepare cellulose nanocrystals, cellulose nanofibrils, lignin nanoparticles, and nanocarbons at a 1:1:1:1 mass ratio. The transportation of all consumables was considered by assuming a transportation distance of 100 km. Detailed inventory data and calculation procedures are provided in the Supplemental Text.

### 2.10. Statistical analysis

Statistical analyses of variance, regression coefficients, and Spearman's rank correlation coefficient were accomplished using Superior Performance Software System (SPSS version 16.0, Inc., Chicago, IL). Pair-wise comparisons were conducted between two measurements using the Student's *t*-test. The line graph, histogram, and regression analysis for the best-fit curve were generated using Origin 2021 software (Microcal Software, Northampton, MA). The average values were calculated from the original triplicate measurements for these analyses.

## 3. Results

### 3.1. Substantial bioethanol production and distinct lignocellulose residues

By employing 1-, 3- and 5-year-old classic bamboo (*Phyllostachys edulis*) plants, termed Y1, Y3, and Y5, respectively, we previously conducted fully green-like (steam explosion followed by green liquor) pretreatments with lignocellulose substrates to enhance biomass saccharification and bioethanol conversion [30]. This study extended the estimation of total sugars (hexoses and pentoses) yields released from both two-step pretreatments and sequential enzymatic hydrolyses in three bamboo samples raised by 12–18 folds relative to the raw materials (Figs. 1 and S1; Table S1). Based on the average xylose-ethanol conversion rate [47], the total ethanol yields could be upgraded by 11–14 fold. The Y1 sample showed significantly higher total sugars and bioethanol yields than the Y3 and Y5 samples at $p < 0.05$ levels ($n = 3$), mainly due to its lower lignin content and cellulose crystallinity, which facilitated more efficient enzymatic saccharification and released greater total sugars. Notably, global bioethanol yields were assessed as $1.35 \times 10^9$, $1{,}17 \times 10^9$, and $0.97 \times 10^9$ ton per year by calculating the total global bamboo production harvested after one, three and five years of growth (Table S1), revealing that short-life (Y1) bamboo is advantageous for efficient bioethanol productivity under green-like processes.

Owing to the highly-crystalline cellulose assembly and rich lignin deposition in bamboo tissues, approximately 11%–16% enzyme-undigested residues of total dry biomass were obtained from the ethanol biorefinery (Fig. 1; Table S2). In comparison, the undigested residues consisted of 21%–27% lignin, 3%–6% cellulose, and 2%–3% hemicellulose; however, the Y1 residue contained significantly less cellulose and lignin than the Y3 and Y5 samples at $p < 0.05$ (Fig. S2). Furthermore, Y1 residue showed relatively lower cellulose crystalline index (CrI) and degree of polymerization (DP) values, consistent with significantly reduced cellulose CrI and DP values in the raw material (Fig. S3A and B). Compared with the raw materials, all enzyme-undigested residues showed an average increase of 35% in cellulose CrI and a 61% reduction in cellulose DP, indicating that the residual cellulose should become more crystalline and less polymerized after enzymatic hydrolysis. These structural characteristics should be favorable for preparation of cellulose nanomaterials. In terms of the composition of three lignin monomers (H, S, and G), the undigested residues contained a predominately reduced H-monomer level by 38% with unaltered G-monomer content, leading to a relatively increased S-monomer content of 26% (Fig. S3C), indicating that distinct lignocellulose residues are conserved from bioethanol biorefinery.

### 3.2. Dimension-reduced cellulose nanofibrils and nanocrystals

As the enzyme-undigested residues contain highly-crystalline cellulose fibers, high pressure homogenization at 60 MPa was performed to generate CNFs after lignin removal by a two-step alkali extraction (Fig. 2A). Under previously-established Atomic Force Microscope (AFM) [17,32], the CNFs derived from the enzyme-undigested residues exhibited rougher surfaces with deep defects, whereas the raw materials exhibited relatively smooth and flat surfaces, because their cellulose microfibrils were tightly embedded within the intact lignin and hemicellulose matrix, resulting in limited fibrillation and fewer surface defects before enzymatic or mechanical disintegration. The average defects' depths were then determined from 30 randomly-selected CNFs, and three residue samples respectively showed the average depths at 3.14 nm, 2.41 nm and 2.17 nm with the average distances of two defects at 76.23 nm, 91.74 nm and 92.35 nm (Fig. 2B and C). Although the defect was not detectable in raw materials, the average CNF diameters were determined at 2.83 nm, 3.42 nm, and 3.58 nm, whereas the three residue samples exhibited diameters of 4.99 nm, 5.91 nm, and 6.09 nm (Fig. 2D). Hence, the enzyme-undigested residues can produce notably length-reduced CNFs with considerable defect accumulation.

Moreover, classic acid catalysis was performed to generate CNCs (Fig. 2E), with rod-like acicular nanoparticles observed as typical CNCs; however, their geometrical dimensions varied significantly (Fig. 2F and G). This rod-like morphology is consistent with previous reports showing that such elongated CNC structures exhibit high aspect ratios, which enhance their mechanical reinforcement, dispersibility, and suitability as building blocks for advanced nanocomposites [48]. Based on measurements of 100 randomly-selected CNCs, the average lengths of CNCs prepared from the Y1, Y3, and Y5 enzyme-undigested residues were 138.19, 148.37, and 206.94 nm, representing reductions of 9.4%, 16.2%, and 26.8% relative to their raw materials (152.46, 177.16, and 282.57 nm). The TEM observations further revealed the similar CNC sizes as observed by AFM (Fig. S4), confirming that the Y1 residue could produce desirable nanomaterials such as the smallest CNFs and shortest CNCs among all samples examined.

### 3.3. Ultrafine lignin nanoparticles

With respect to the bamboo tissues rich in lignin deposition, this

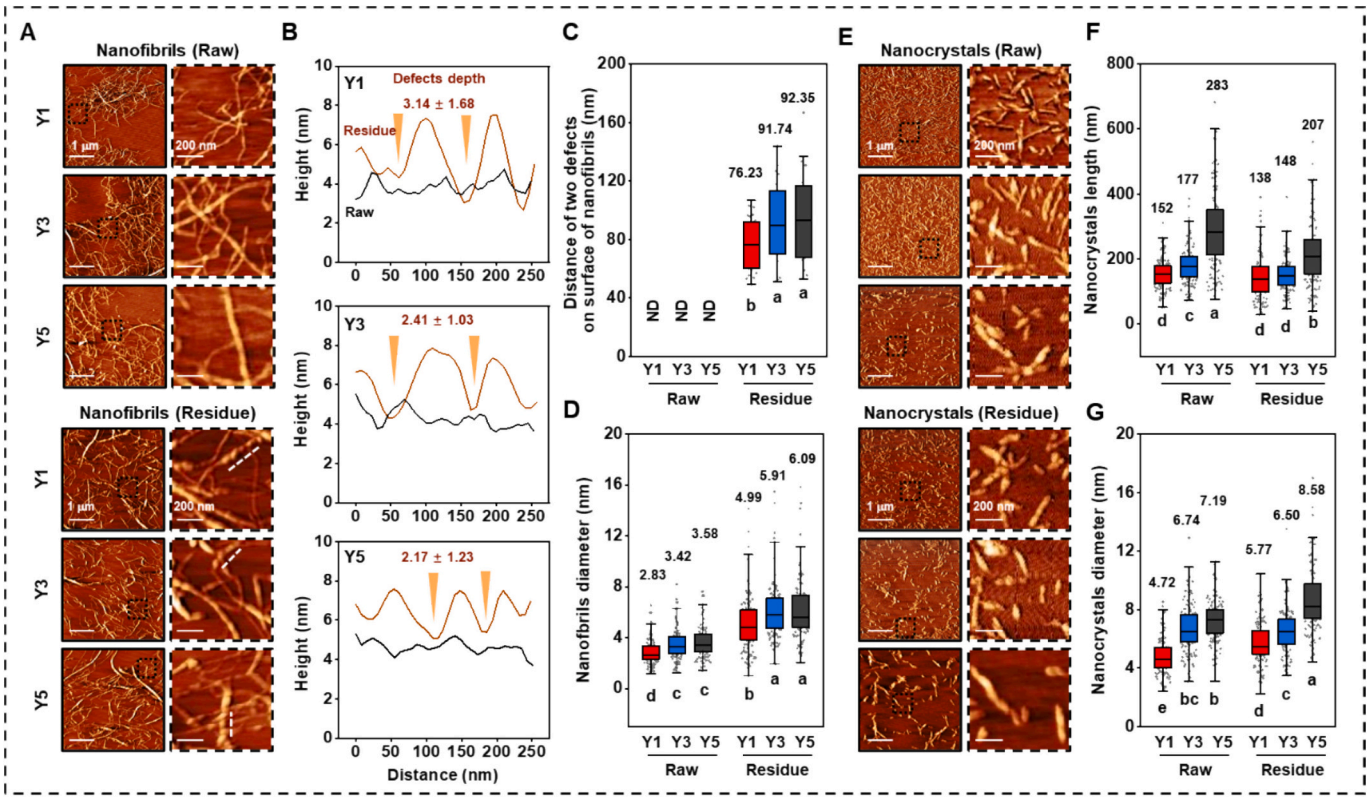


**Fig. 2.** Distinct cellulose nanofibrils and nanocrystals generated from different-year-old bamboo samples. (A) Atomic Force Microscopy (AFM) images of cellulose nanofibrils; (B) cross profiles corresponding to white lines in (A) to illustrate alternate breakpoints for nanofibrils-defect depths of the enzyme-undigested residues (Residue) ($n = 30$); (C) the average distance between two defects on the surfaces of cellulose nanofibrils as highlighted in (A), ND as not detectable; (D) average diameter of cellulose nanofibrils by randomly-selected samples ($n = 100$); (E) AFM images of cellulose nanocrystals; (F, G) average length and diameter of cellulose nanocrystals ($n = 100$); Lowercases (a, b, c) as multiple significant differences among Y1, Y3 and Y5 samples by LSD test at $p < 0.05$.

study integrated acid hydrolysis or ethanol precipitation with glycerol-microwave treatment to generate LNPs from raw materials, two-step pretreatment supernatants, and enzyme-undigested residues (Fig. 3A). The raw materials and pretreatment supernatants generated core-shell-like LNPs, whereas the undigested residues produced highly condensed LNPs (Figs. 3B-D and S5). By measuring the average diameters of 100 randomly selected LNPs, extremely small LNPs were found in the undigested-residues, with diameters reduced by 73%–87% compared to the other two lignin resources (Fig. 3E-G). The formation of such ultrafine LNPs indicates enhanced lignin depolymerization and molecular fragmentation during pretreatment, which facilitates higher surface reactivity and greater potential for use in high-performance nanocomposites and catalytic applications [49]. Notably, the LNPs of the residue samples exhibited normal distributions with small variations in average diameters, whereas the LNPs diameters varied largely in the raw materials or pretreatment supernatants. More importantly, the Y1 samples generated the smaller LNPs with the narrowest polydispersion index, and the Y1 undigested-residue could even produce the smallest LNPs with average diameter reduced by 92%–96% to date, compared to the previously-generated LNPs from other biomass resources (Fig. 3K; Table S3).

To understand the minimal LNPs generated from enzyme-undigested residues, the lignin monomer compositions were characterized. The relative abundances of lignin monomers in raw materials, pretreatment supernatants, and enzyme-undigested residues were quantified using the nitrobenzene oxidation method. The results showed that Y1 lignin consistently exhibited a higher guaiacyl (G) monomer content than Y3 and Y5 across all lignin fractions, with G-unit proportions of 48.02%, 45.76%, and 42.63% in the enzyme-undigested residues, respectively (Fig. 3H). As shown in Fig. 3I, the S/G ratio of lignin in the enzyme-undigested residues was consistently lower in Y1 relative to Y3 and Y5, suggesting a guaiacyl-enriched structural feature in Y1. This compositional difference may influence the intermolecular interactions governing lignin nanoparticle formation. Functional groups of lignin were detected in the benzene ring and side chains by Fourier Transform Infrared Spectrometer (FTIR) analyses, including the phenylpropane skeleton at 1508 $cm^{-1}$, the syringyl unit at 1120 and 1329 $cm^{-1}$, and the guaiacyl-unit-based vibration at 1270 $cm^{-1}$ (Fig. S6; Table S4), indicating that the LNPs dimensions of three lignin resources were distinctively affected by the proportions and interlinkages of three monomers. Correlation analysis showed that the H- and G-monomer proportions were negatively correlated with the LNPs diameters of the residue samples, whereas the S-monomer proportions was positively correlated with the LNPs diameters of the raw materials and pretreatment supernatants (Fig. 3J), suggesting that lignin monomer compositions should be associated with the nanoparticle formation. The mechanism model is thus proposed to explain how the nanoparticle formation is regulated by the combined effects of H-, G-, and S-unit distribution rather than the abundance of a single monomer (Fig. S7). As the H- and G-rich lignin contain less methoxy substituents than S-rich lignin, it may reduce steric hindrance to facilitate intermolecular aromatic interactions during solvent shifting [49–51], which should promote rapid nucleation and suppress excessive particle growth, ultimately resulting in smaller lignin nanoparticles formation as observed [52].

### 3.4. Porosity-raised graphitic nanocarbon

Given that the Y1 sample produced the smallest LNPs from the enzyme-undigested residue, this study attempted to generate porous carbon by operating thermal-chemical activation and conversion

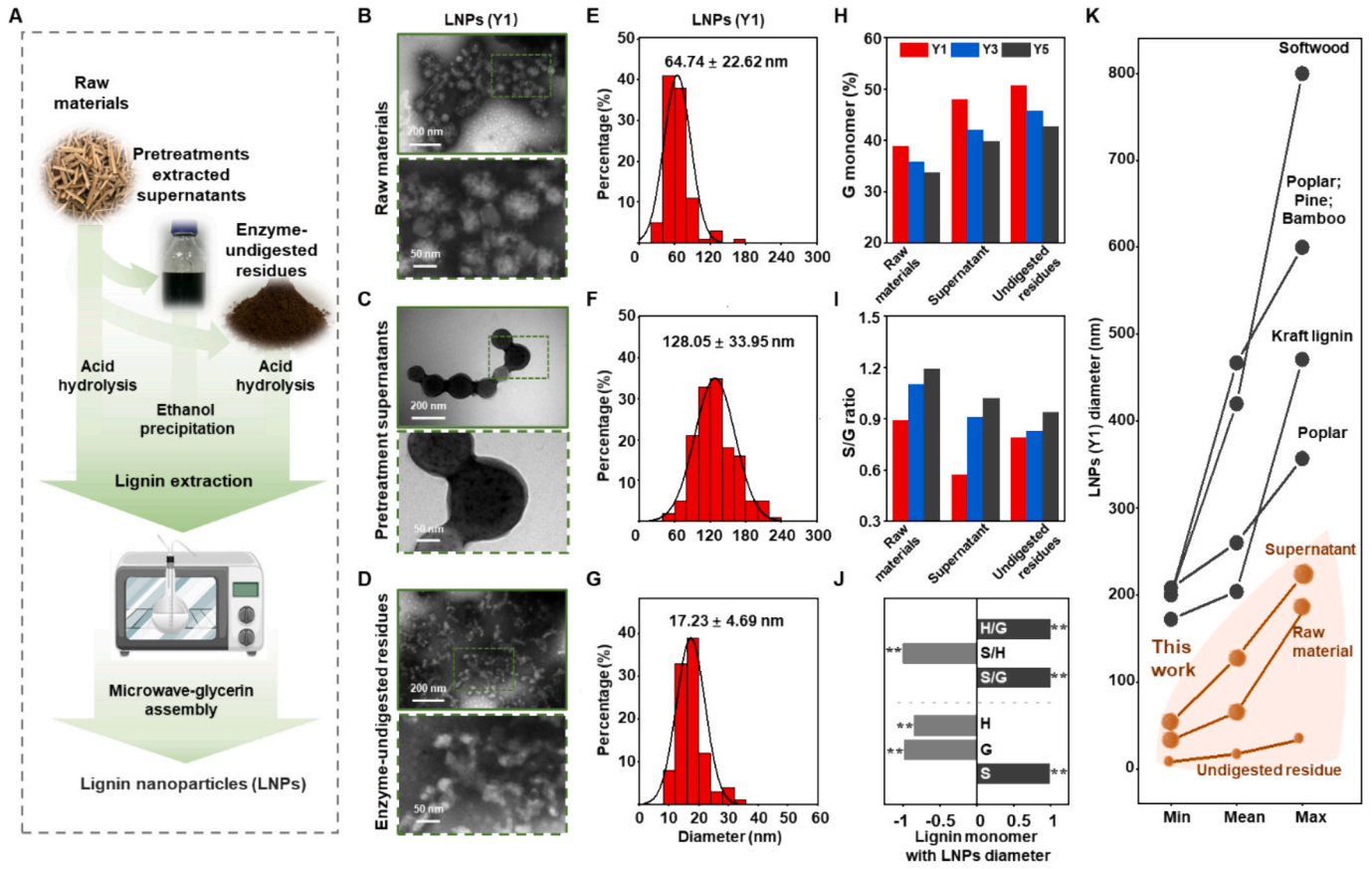


**Fig. 3.** Distinct lignin nanoparticles (LNPs) generated from bamboo samples. (A) Flowchart for generations of LNPs from three lignocellulose resources; (B-D) TEM images of LNPs; (E-G) histograms for diameter distributions of LNPs by using randomly-selected Y1 bamboo samples ($n = 100$); (H, I) lignin guaiacyl (G) monomer proportion and S/G ratio of three lignocellulose resources; (J) correlation analyses between LNPs diameters and lignin monomer levels/ratios in all bamboo samples examined ($n = 9$), ** As significant correlation at $p < 0.01$ level; (K) comparison of LNPs diameters among the Y1 bamboo samples and previously-reported ones from other biomass resources.

(Fig. 4). The optimal reaction conditions were initially determined by using different proportions of chemical ($K_2FeO_4$) at various incubation temperatures (Fig. S8). Using BET assay, the largest specific surface area was detected in the carbon sample generated from $K_2FeO_4$ (1:2, w/w) activation at 800 °C, suggesting that the strong oxidative and catalytic properties of $K_2FeO_4$ promoted pore development and graphitization, while the lower lignin content and reduced cellulose polymerization degree of the Y1 sample facilitated the formation of a more porous carbon framework. All Y1 samples displayed a diffraction peak at 26.5°, attributed to typical graphite carbon by X-ray diffraction (XRD) analyses (Fig. S8C and S8D). Meanwhile, the ($I_D/I_G$) ratios between the D (~1350 $cm^{-1}$) and G peaks (~1580 $cm^{-1}$) from Raman scanning were calculated to account for the graphite degree of carbons (Fig. S8E and S8F). However, a sharp 2D band was only observed in the carbon with $I_D/I_G$ at 0.42, indicating a high degree of graphitization and fewer graphene layers (Fig. S8F).

Under optimal thermal/chemical conditions, the carbon derived from Y1 enzyme-undigested residue exhibited a markedly pore-rich surface morphology, whereas the carbon obtained from the raw bamboo material displayed fewer pores (Fig. 4A). The abundant pore structures facilitate electrolyte penetration and provide a larger number of electrochemically active sites. The degree of graphitization of the carbon samples was characterized by XRD and Raman spectroscopy, and their textural properties were further evaluated by $N_2$ adsorption-desorption measurements at 77 K. The corresponding isotherms and pore size distributions are presented in Fig. 4B and C, with detailed adsorption parameters summarized in Table S6. The porous carbon derived from Y1 enzyme-undigested residue exhibited continuous $N_2$ adsorption in both the low and medium relative pressure pressures ($0 < P/P_0 < 0.1$, $0.1 < P/P_0 < 0.5$) and displayed a distinct hysteresis loop at higher relative pressures ($0.5 < P/P_0 < 1$), corresponding to a mixed type I/IV adsorption isotherm (Fig. 4B). Moreover, the enzyme-undigested residue carbon exhibited a large BET surface area of 2856 $m^2\ g^{-1}$ and a large total pore volume of 1.76 $cm^3\ g^{-1}$, accompanied by a narrow pore size distribution centered at approximately 3.40 nm, was assigned to mesopores (Fig. 4C, Table S6). The combination of a high specific surface area and an optimized mesopore-micropore distribution is favorable for electrolyte infiltration and ion adsorption, thereby enhancing charge storage capability. In contrast, the carbon prepared from the Y1 raw material exhibited a typical type I adsorption-desorption isotherm, characterized by a sharp adsorption inflection at low relative pressures and a well-defined plateau, indicative of a predominance of microporous structures (Fig. 4B). This sample possessed a narrow pore size distribution centered at 2.05 nm, together with a relatively lower BET specific surface area of 1669 $m^2\ g^{-1}$ and a smaller total pore volume of 0.97 $cm^3\ g^{-1}$ (Fig. 4C, Table S6). In Fig. 4D, the $I_D/I_G$ ratios of the carbons derived from Y1 raw material and enzyme-undigested residues were 0.88 and 0.87, respectively. The comparable $I_D/I_G$ values indicate that the catalyst was highly effective in promoting carbonization and graphitization in both samples, leading to a similar overall degree of graphitic ordering. Notably, the carbon derived from enzyme-undigested residues exhibited a slightly lower $I_D/I_G$ ratio, suggesting a modestly increased graphitization degree, which may be attributed to the higher crystallinity of cellulose retained in the residues and its more ordered carbon framework formed during thermal conversion.

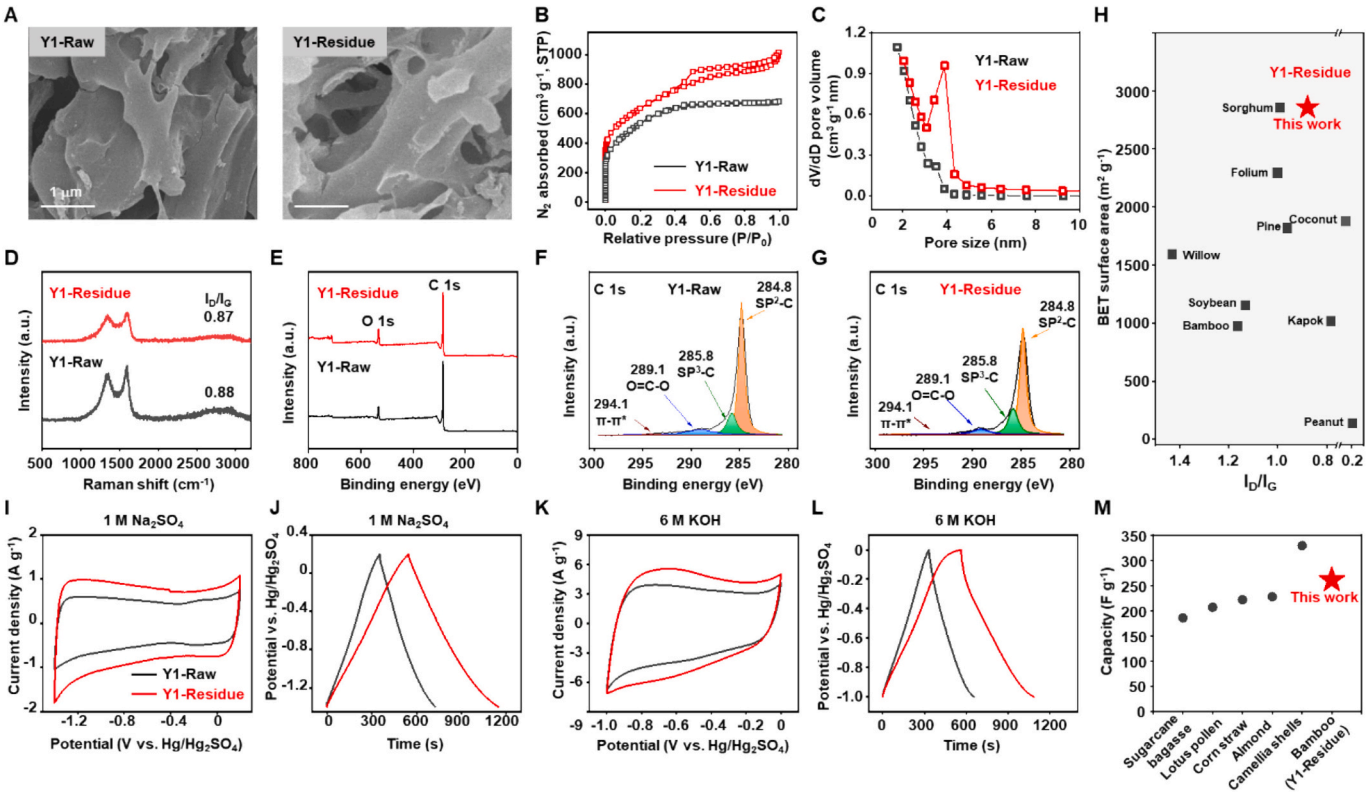


**Fig. 4.** Characterization of the nanocarbons generated from Y1 bamboo. (A) SEM images of the porous nanocarbons; (B) $N_2$ absorption-desorption isotherms; (C) Pore size distribution; (D) Raman scan profiling for two typical D- and G-peaks; $I_D/I_G$ as ratio of two peaks; (E) XPS spectra for two typical peaks of C- and O-elements; (F, G) high resolution C 1s spectrum of nanocarbons in raw and residue samples; (H) comparison of the BET surface areas and $I_D/I_G$ ratios of nanocarbons among the Y1 bamboo sample and previously-reported ones from other biomass resources. (I, K) Cyclic voltammetry curves; (J, L) galvanostatic charge/discharge curves; (M) comparison of the capacity (F $g^{-1}$) of residue sample with the previous reports from other biomass resources.

Based on the XPS elemental assay, the Y1 undigested-residue produced nanocarbons containing less carbon (C) at 84.1%, with a relatively higher proportion of oxygen (O) at 11.6%, indicating more oxygen-containing functional groups as active sites (Figs. 4E-G and S9; Table S5). Accordingly, the Y1 residual sample showed a higher proportion of nitrogen (N) relative to its raw material sample, possibly owing to the presence of the cellulase enzymes employed for biomass saccharification. XPS profiling exhibited one sharp peak at 284.6 eV corresponding to graphite (C-C), with four other individual peaks identified as $sp^2$-bonded carbon (284.8 eV), $sp^3$-C (285.8 eV), O=C-O (289.1 eV) and a satellite peak of π–π* (294.1 eV). The abundant oxygen- and nitrogen-containing functional groups revealed by XPS likely contributed to additional pseudocapacitance through reversible redox reactions at the electrode–electrolyte interface, thereby enhancing the overall capacitive performance of the nanocarbon materials [42]. Meanwhile, this study obtained carbons from the Y3 and Y5 bamboo samples; however, the Y1 sample could generate porous carbon with the largest BET surface area of 2865 $m^2$ $g^{-1}$ (Table S6). Furthermore, compared to the carbons previously generated from other major biomass resources reported before, the Y1 undigested-residue sample had the second-highest BET surface area (Fig. 4H; Table S7).

### 3.5. Improved supercapacitor performance

Two reaction systems were applied using 1 M $Na_2SO_4$ and 6 M KOH aqueous electrolytes (Fig. 4I-L) to test the electrochemical performance of the porous nanocarbons generated from Y1 samples. Cyclic voltammetry (CV) curves were obtained at different sweep rates (Figs. 4I, K, and S10–13). All curves displayed quasi-rectangular shapes, accounting for the good characteristics of the double-layer capacitor; however, the undigested-residue sample showed the highest current response at different scan rates (Fig. S14). With the sweep speed increased to 100 mV $s^{-1}$, the residue samples maintained a perfect rectangular shape, while the Y1 residue still displayed the rectangular-like curves even at 150 mV $s^{-1}$ in both electrolytes. Galvanostatic charge-discharge (GCD) tests conducted with six samples exhibited a typical inverted "V" shape, indicative of classic capacitive response and fast charge transfer; however, the Y1 residue persisted the longest discharging time for the highest specific capacitance in two electrolyte systems (Fig. 4J and L). The specific capacitances were evaluated by the discharge times at different current densities, and the Y1 residue had the highest specific capacitances at 189 F $g^{-1}$ (1 M $Na_2SO_4$) and 261 F $g^{-1}$ (6 M KOH) among all the samples examined (Fig. S14C and S14F) and possessed the second highest capacitance among the carbons generated from other biomass resources (Fig. 4M; Table S8), suggesting that its highly graphitized structure, larger specific surface area, and abundant oxygen-containing functional groups provided more active sites and facilitated rapid ion transport during charge-discharge processes.

### 3.6. Increased $CO_2$ adsorption and bioeconomic benefits

Using the porous carbon of the Y1 sample, this study measured $CO_2$ adsorption capacities at two representative temperatures (Fig. 5A and B). The residue sample showed consistently higher $CO_2$ adsorption capacities than the raw material incubated at 0 °C and 25 °C. However, the raw material and undigested-residue samples had a relatively lower $CO_2$ adsorption capacity at 25 °C, suggesting that such $CO_2$ adsorption is an exothermic process. Analysis of the pore size distribution revealed that the Y1-derived carbon predominantly contained micropores (<2 nm), which are favorable for $CO_2$ adsorption due to enhanced surface confinement and interaction energy (Fig. 4C; Table S6). Notably, the Y1 residue sample displayed the second-highest $CO_2$ adsorption capacity

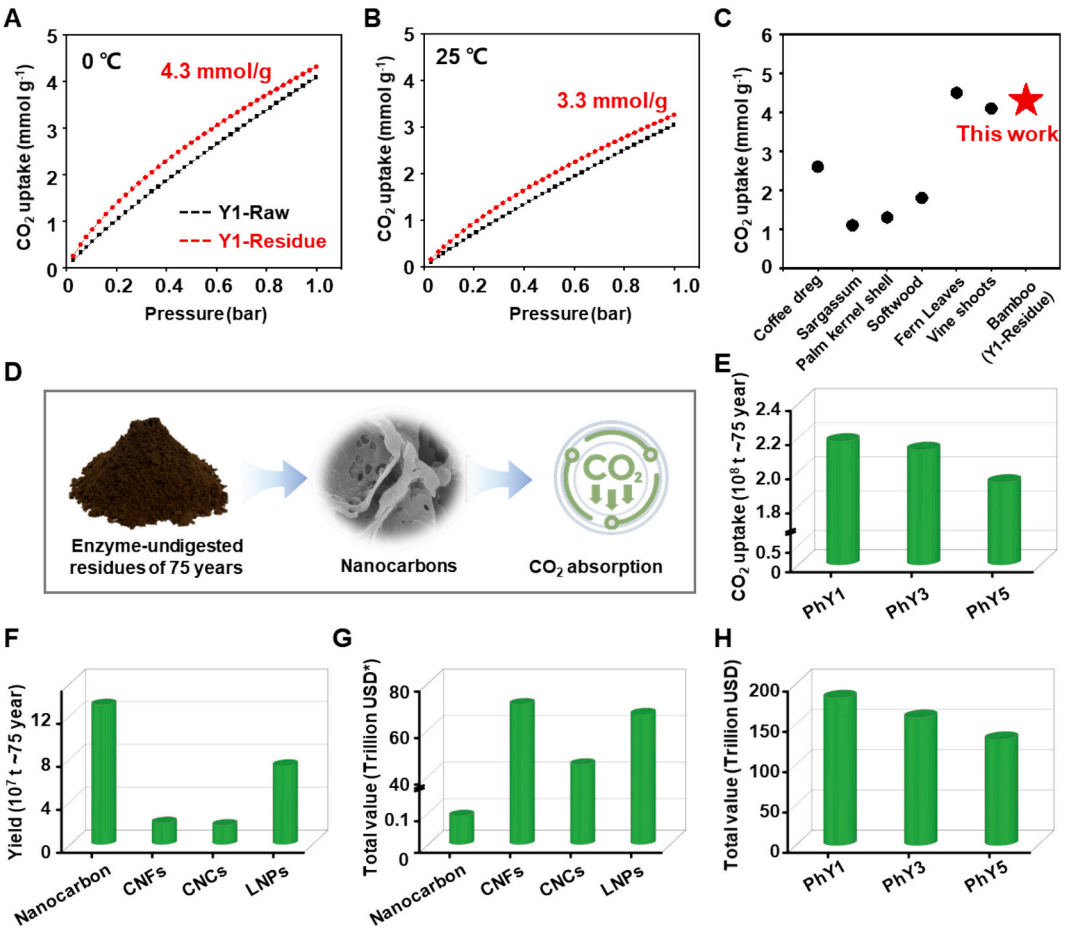


**Fig. 5.** $CO_2$ adsorption of the nanocarbons and global estimation of potential profitable values of advanced nanomaterials for 75 years (2025–2100) bamboo harvest. (A, B) $CO_2$ adsorption of nanocarbons generated from Y1 raw material and enzyme-undigested residue at 0 °C and 25 °C under 1 bar pressure; (C) comparison of the $CO_2$ adsorption between the Y1 residue sample and the previously-reported ones from other biomass resources; (D) the enzyme-undigested residues of 75 years bamboo harvest applied to prepare nanocarbons for global $CO_2$ absorption; (E) estimation of total global $CO_2$ absorption of different-year-old bamboo enzyme-undigested residues; (F, G) global evaluations of total advanced nanomaterials yields and profitable values of Y1 enzyme-undigested residues; (H) profitable values of advanced nanomaterials from the enzyme-undigested residues of different-year-old bamboos. USD as United States Dollar.

among the carbons as previously generated from other biomass resources (Fig. 5C; Table S9). In line with the biorefinery concept, the integrated bamboo-based system not only converts lignocellulosic residues into bioethanol but also enables the green production of high-value nanomaterials such as CNFs, CNCs, LNPs, and nanocarbons, thereby maximizing resource utilization and minimizing waste generation. Based on global bamboo growth for 75 years (2025–2100), this study estimated total $CO_2$ adsorption capacity of the nanocarbons generated from the enzyme-undigested residues after bioethanol biorefinery (Fig. 5D), and the maximum $CO_2$ adsorption ($2.18 \times 10^8$ t) was evaluated from Y1 bamboo harvest compared to the Y3 and Y5 ones (Fig. 5E). Meanwhile, total yields and economic benefits of four nanomaterials were respectively estimated from the Y1 bamboo harvest (Fig. 5F and G). In comparison, the CNFs and LNPs were of relatively higher profit values at $7.10 \times 10^{13}$ and $6.68 \times 10^{13}$ USD according to current market prices (Fig. 5G; Table S10). Despite of the lowest profit value, the nanocarbons had the highest yield at $1.30 \times 10^8$ t for $CO_2$ adsorption. In addition, total profit value of the four nanomaterials derived from Y1 bamboo could reach $1.83 \times 10^{14}$ USD over the 75-year assessment period, corresponding to approximately $1.81 \times 10^3$ USD per metric ton of harvested bamboo biomass, which remained much higher than those of the Y3 and Y5 bamboo (Fig. 5H).

### 3.7. Reduced $CO_2$ emission and environmental impacts

Considering the substantial bioethanol production followed by advanced nanomaterials generation from short-life (Y1) bamboo processes, this study conducted the life cycle assessment (LCA) to estimate potential reduction of $CO_2$ emission via rapid carbon capture and long-term carbon storage (Fig. 6A). By setting up a "cradle-to-gate" LCA boundary, about 1 kg of bamboo was defined as the functional unit for all essential evaluations (Fig. 6A; Tables S11–18). Total $CO_2$ emissions from the major stages of Y1 bamboo conversion were estimated and compared with the traditional fossil-gasoline production, as gasoline represents the primary fossil-based fuel currently dominating global transportation energy consumption and serves as a standard benchmark for evaluating bioethanol's carbon reduction potential. As a result, approximately 1 kg bioethanol conversion briefly produced 0.80 kg $CO_2$ -eq as the globe warming potential (GWP), whereas 1 kg gasoline could produce 1.54 kg $CO_2$ -eq (Fig. 6B). Of the four advanced nanomaterials generated from enzyme-undigested residues, the nanocarbon conversion had the lowest GWP value of 0.29 kg $CO_2$ -eq/kg, whereas the CNFs construction had the highest value (Fig. 6G). Based on the estimated cumulative Y1 biomass yields of 75 years, the total bioethanol yield was calculated to be close to $2.06 \times 10^9$ t, which could replace $6.14 \times 10^8$ t gasoline based on equal calorific value between cellulosic-ethanol and petrol-gasoline. Meanwhile, total $CO_2$ emission was assessed up to $2.96 \times 10^9$ t from both bioethanol conversion and four types of nanomaterials

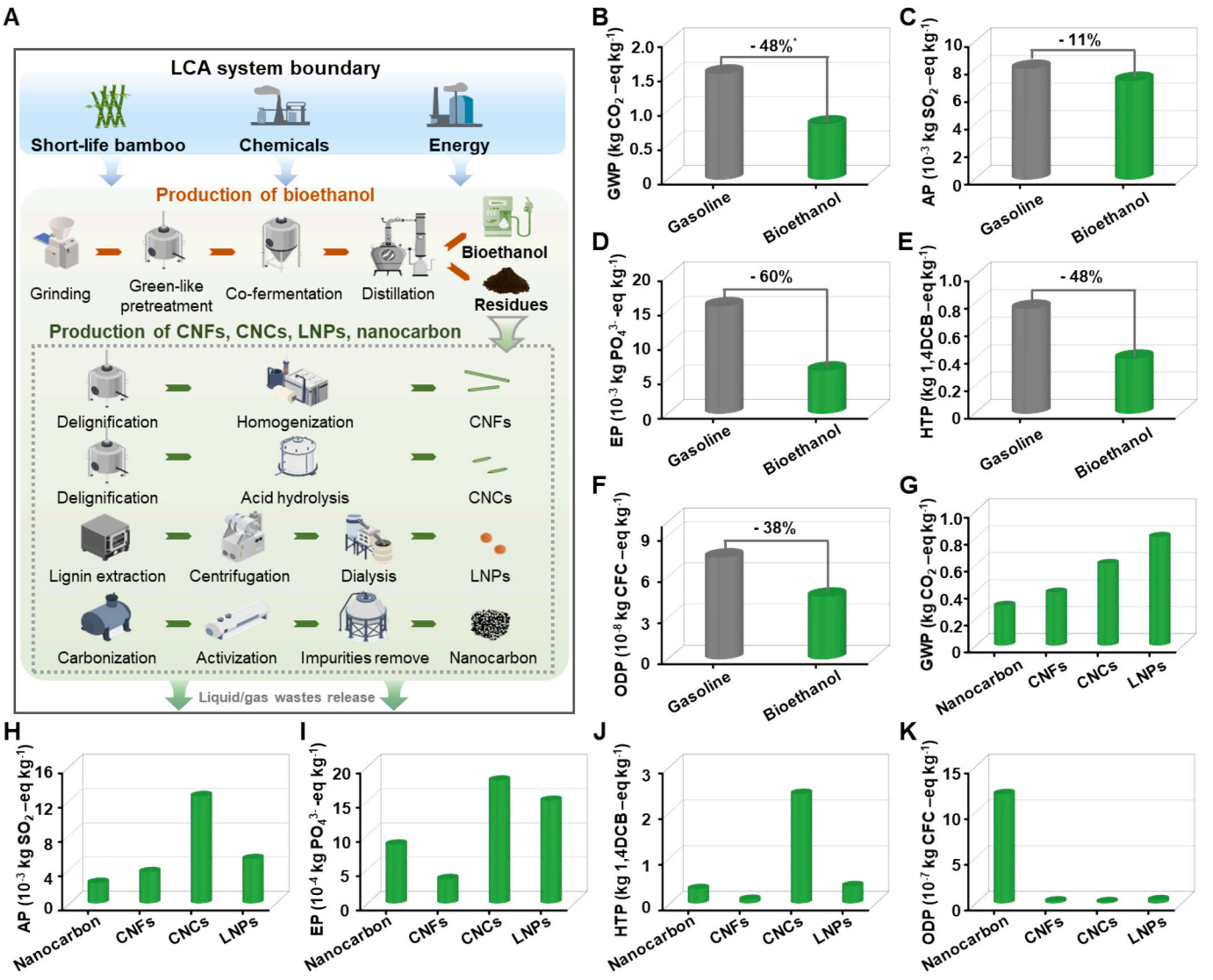


**Fig. 6.** Life cycle assessment (LCA) of bioethanol and nanomaterials production. (A) Systems boundaries for bioethanol and nanomaterials (CNFs, CNCs, LNPs, nanocarbon) including the background system (production of related materials and energy) and the foreground system (production processes of the products); (B-F) total environmental impacts from 1 kg bioethanol conversion examined in this study and 1 kg gasoline production from industry; (G-K) environmental impacts from four nanomaterials generations using 1 kg enzyme-undigested residue at equal parts of total (1:1:1:1); GWP (global warming potential), AP (acidification potential), EP (eutrophication potential), HTP (human toxicity potential), ODP (ozone depletion potential); *As reduced percentage by subtraction between gasoline and bioethanol values divided by gasoline value.

generations at the equal part (1:1:1:1) of total enzyme-undigested residues, whereas the gasoline production would emit 5.47 × $10^9$ t $CO_2$ based on the equivalent energy output of bioethanol and gasoline (Fig. 7). As 5.15 × $10^{11}$ t of $CO_2$ emissions could increase the globe surface temperature by 1 °C [53], the Y1 bamboo growth for 75 years would maintain global warming relief via replacement of petrol-gasoline.

Furthermore, this study assessed the distinct environmental factors on bioethanol conversion and nanomaterials generation from Y1 bamboo harvest (Tables S11–18). As a result, the four major environmental factors showed consistently reductions from bioethanol production by 11%–60% compared to the gasoline (Fig. 6C-F). For four nanomaterials generation, the nanocarbon had the least impact on eutrophication potential and human toxicity potential, whereas the LNPs conversion showed a relatively lower effect on acidification potential and ozone potential (Fig. 6H-K). Notably, even though the generation of four types of nanomaterials led to reduced carbon emissions (Fig. 6G), they could partially substitute traditional materials to upgrade bioeconomic benefits from global bamboo growth for 75 years as described.

## 4. Discussion

Given that bamboo affords substantial lignocellulose for biofuels and bioproducts, biomass processes principally employ mature plants (with five years of growth) [29,54]. However, this study explored the multiple advantages of the cascading utilization of the short-life (one-year-old/Y1) bamboo by maximizing global bioethanol production and generating advanced nanomaterials (Fig. 1).

First, bamboo sustainably regenerates after one year of harvest, and the Y1 plant has the fastest growth rate for biomass productivity. Second, even under green-like biomass pretreatments, Y1 bamboo could globally produce the maximum fermentable sugars for bioethanol sustainability, as determined by the largest quantity of bamboo harvested per year and the best quality of lignocellulose examined from remarkably improved recalcitrant properties such as less-lignin deposition and

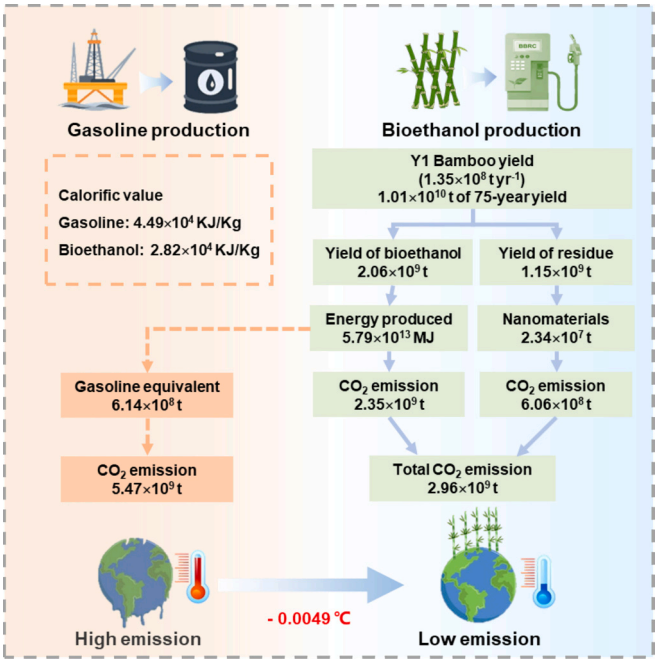


**Fig. 7.** Evaluation of total $CO_2$ emission potential for global temperature relief via bioethanol replacement of gasoline until 2100.

lower-DP-cellulose assembly among different-year-old bamboo plants. Third, although the extreme chemical pretreatments could effectively reduce lignocellulose recalcitrance in older bamboo plants, they could not avoid a cascading negative impact on bioeconomic profits and environmental benefits such as high-cost processes, secondary-waste release, and low-value bioproduction. Despite these advantages in biomass conversion and cascading biorefinery, the industrial productivity of Y1 bamboo may still face the challenges related to mechanical strength, harvesting logistics, and integration with existing bamboo-processing systems. Nevertheless, as the Y1 bamboo is of either relatively lower lignocellulose recalcitrance favor for biochemical conversion or rapid regeneration sufficient for biomass supply, it could serve as a complementary feedstock during routine thinning and stand management.

Although diverse lignocelluloses are increasingly being used to generate advanced nanomaterials, biomass recalcitrance naturally restricts the separation, extraction, and catalysis of wall polymers [55,56]. However, the recalcitrance-reduced lignocellulose of Y1 bamboo is not only digestible for sustainable hexoses at high yields, but the enzyme-undigested residue is also convertible for advanced nanomaterials with extremely high values. As the remaining cellulose residue of Y1 bamboo has a much lower polymerization degree (<350 DP) and high crystalline index (>70 CrI), it could be transformed into either CNFs with smaller diameters or CNCs with shorter lengths, as compared with older bamboo or major bioenergy crops as previously examined. Compared with their raw materials, the enzyme-undigested residues retain the cellulose substrates with approximately 35% higher CrI and 61% lower DP values (Fig. S3A and B). These cellulose feature changes may modify the fibrillation behavior during homogenization, resulting in a slightly larger apparent CNF diameter, whereas sulfuric acid hydrolysis could primarily shorten the cellulose crystalline domains with little change in CNC diameters [17,18,57,58]. The remaining lignin residue of Y1 bamboo could even generate the smallest LNPs among the most lignocellulose substrates as previously reported, which should be mainly due to its distinctive lignin monomer composition such as relatively higher H- and G-unit contents as assumed (Fig. S7). Considering the enzyme-undigested residue of the Y1 bamboo consists of both DP-reduced cellulose nanofibrils and molecule/mass-reduced lignin, it is thus thermally converted into the desirable graphitic nanocarbon with the largest specific surface area, leading to a larger current response and higher specific capacitance. In addition, the nanocarbon of the Y1 sample exhibited a relatively higher $CO_2$ adsorption for carbon capture.

Although cellulosic ethanol is an excellent additive to petrol-fuels for reducing net carbon emissions, critical challenges remain about the sustainability of economic profits and the control of global warming [59,60]. Based on the LCA implementation of rapid carbon capture and long-term carbon storage, an integrative reduction in either total $CO_2$ emissions or major environment impacts was respectively estimated from the full lignocellulose utilization of Y1 bamboo with zero-biomass release (Fig. 7).

Overall, the integration of sustainable bioethanol production, high-value nanomaterials and robust environmental performance has demonstrated that short-life bamboo represents a promising renewable feedstock for future low-carbon lignocellulosic biorefineries. To evaluate the influence of market-driven product allocation on the environmental performance of the proposed cascading biorefinery, sensitivity analyses could be further conducted by assuming dominant production of CNFs, CNCs, LNPs, or nanocarbon. Although the absolute environmental impacts are varied slightly among different allocation scenarios, the overall environmental advantages of the Y1 bamboo biorefinery remain unchanged (Fig. S15, Table S19). Those results have thus revealed that the LCA conclusions are robust across different product allocation scenarios in product distribution to support for the practical applicability of the proposed cascading utilization strategy.

## 5. Conclusions

This study demonstrates that short-life bamboo enables an integrative green-like process for high-yield bioethanol production and advanced nanomaterial fabrication, achieving full lignocellulose utilization with zero-biomass release. Particularly, reduced biomass recalcitrance has not only enhanced enzymatic saccharification, but it has also facilitated the fabrication of high-quality cellulose nanomaterials, ultrafine lignin nanoparticles, and graphitic nanocarbon with superior electrochemical performance and $CO_2$ adsorption capacity. The life-cycle assessment has further confirmed that this cascading utilization strategy could substantially reduce carbon emissions and multiple environmental impacts. These findings support short-life bamboo as a sustainable, recyclable biomass resource and suggest that cascading biorefinery of rapidly renewable plants may offer a practical pathway toward agricultural carbon neutrality.

## CRediT authorship contribution statement

**Hairong Gao:** Writing – original draft, Visualization, Software, Methodology, Investigation. **Boyang He:** Software, Methodology, Investigation. **Yixiang Wang:** Writing – original draft, Visualization, Software, Methodology, Investigation. **Hao Peng:** Software, Investigation. **Peng Liu:** Software, Investigation. **Yongtai Wang:** Software, Investigation. **Yanting Wang:** Software, Funding acquisition. **Qiang Li:** Software, Funding acquisition. **Zhi Qi:** Software, Funding acquisition. **Hua Yu:** Supervision, Project administration, Methodology, Funding acquisition. **Xinchun Lin:** Supervision, Project administration, Methodology, Funding acquisition. **Liangcai Peng:** Writing – review & editing, Supervision, Methodology, Funding acquisition, Conceptualization.

## Declaration of competing interest

The authors declare that they have no known competing financial interests or personal relationships that could have appeared to influence the work reported in this paper.

## Acknowledgements

We thank Dr. Feifei Cao for the kind assistance in the supercapacitor test and valuable advice on data analysis. This work was in partial supported by the National Natural Science Foundation of China (32470273 to L. P, 32101701 to Y. W), the Initiative Grant of Hubei University of Technology for High-level Talents (GCC20230001 to L. P), Hubei Provincial Natural Science Foundation of China for Excellent Young Scientists (2024AFA100 to Y·W).

## Appendix A. Supplementary data

Supplementary data to this article can be found online at https://doi.org/10.1016/j.ijbiomac.2026.154286.

## Data availability

Data will be made available on request.

## References

[1] O. Boiral, M.-C. Brotherton, D. Talbot, Achieving corporate carbon neutrality: a multi-perspective framework, J. Clean. Prod. 467 (2024), https://doi.org/10.1016/j.jclepro.2024.143040.
[2] S.G. Fattah, S. Karimi, S. Yuan, Z. Li, M.J. Zohuriaan-Mehr, L. Lin, X. Zeng, B. Han, $CO_2$ utilization and fixation in biomass-derived furanics conversion: thermochemical and electrochemical pathways, Green Energy Environ. 11 (1) (2026) 1–22, https://doi.org/10.1016/j.gee.2025.09.011.
[3] Y. Wang, J. Wen, S. Li, J. Li, H. Yu, Y. Li, X. Ren, L. Wang, J. Tang, X. Zhang, Z. Liu, L. Peng, Upgrading pectin methylation for consistently enhanced biomass enzymatic saccharification and cadmium phytoremediation in rice *Ospmes* site-mutants, Int. J. Biol. Macromol. 262 (2024), https://doi.org/10.1016/j.ijbiomac.2024.130137.
[4] Y. Wang, P. Liu, G.F. Zhang, Q.M. Yang, J. Lu, T. Xia, L.C. Peng, Y.T. Wang, Cascading of engineered bioenergy plants and fungi sustainable for low-cost bioethanol and high-value biomaterials under green-like biomass processing, Sust. Energy Rev. 137 (2021) 110586, https://doi.org/10.1016/j.rser.2020.110586.
[5] S. Lu, L. Sun, Y. Wang, H. Peng, B. He, X. Yuan, Y. Wang, T. Xia, L. Peng, P. Liu, Dual-upgraded biomass saccharification and bioethanol production by cascading peptides interactions with polymers and activating cellulases in bioenergy crops, Renew. Energy 256 (2026), https://doi.org/10.1016/j.renene.2025.124651.
[6] H. Wang, S. Li, L. Wu, W. Zou, M. Zhang, Y. Wang, Z. Lv, P. Chen, P. Liu, Y. Yang, L. Peng, Y. Wang, Semi-overexpressed OsMYB86L2 specifically enhances cellulose biosynthesis to maximize bioethanol productivity by cascading lignocellulose depolymerization via integrated rapid-physical and recyclable-chemical processes, Green Chem. 27 (30) (2025) 9127–9143, https://doi.org/10.1039/D5GC00658A.
[7] P. Jiang, G. Zhao, H. Zhang, T. Ji, L. Mu, X. Lu, J. Zhu, Towards carbon neutrality of calcium carbide-based acetylene production with sustainable biomass resources, Green Energy Environ. 9 (6) (2024) 1068–1078, https://doi.org/10.1016/j.gee.2022.12.004.
[8] T. Li, H. Peng, B. He, C. Hu, H. Zhang, Y. Li, Y. Yang, Y. Wang, M.M.A. Bakr, M. Zhou, L. Peng, H. Kang, Cellulose de-polymerization is selective for bioethanol refinery and multi-functional biochar assembly using brittle stalk of corn mutant, Int. J. Biol. Macromol. 264 (2024), https://doi.org/10.1016/j.ijbiomac.2024.130448.
[9] M. Wang, Y. Wang, J. Liu, H. Yu, P. Liu, Y. Yang, D. Sun, H. Kang, Y. Wang, J. Tang, C. Fu, L. Peng, Integration of advanced biotechnology for green carbon, Green Carbon 2 (2) (2024) 164–175, https://doi.org/10.1016/j.greenca.2024.02.006.
[10] C.B. Xu, J.J. Zhu, H.Z. Yu, H. Yu, Y.Q. Yang, Q.L. Fu, D. Zhan, Y.T. Wang, H. L. Wang, Y.Q. Zhang, T.Q. Li, M.M. El-Sheekh, L.C. Peng, T. Xia, Recyclable cascading of arsenic phytoremediation and lead removal coupled with high bioethanol production using desirable rice straws, Biochem. Eng. J. 168 (2021) 107950, https://doi.org/10.1016/j.bej.2021.107950.
[11] H. Yu, M. Hu, Z. Hu, F. Liu, H. Yu, Q. Yang, H. Gao, C. Xu, M. Wang, G. Zhang, Y. Wang, T. Xia, L. Peng, Y. Wang, Insights into pectin dominated enhancements for elimination of toxic Cd and dye coupled with ethanol production in desirable lignocelluloses, Carbohydr. Polym. 286 (2022) 119298, https://doi.org/10.1016/j.carbpol.2022.119298.
[12] J. Yu, Z. Tang, L. Zhu, B. Gao, J. Hong, Y. Fang, J. Kang, D. Sun, H. Peng, B. He, M. M.A. Bakr, Y. Wang, L. Peng, H. Yu, Low-temperature $ZnCl_2$ activation of distinct *Miscanthus* lignin as highly-porous biochar assembly for efficient removal of organic dyes, tetracycline and Cr(VI), Ind. Crop. Prod. 240 (2026), https://doi.org/10.1016/j.indcrop.2026.122630.
[13] X. Li, J.J. Shen, B.J. Wang, X.L. Feng, Z.P. Mao, X.F. Sui, Acetone/water cosolvent approach to lignin nanoparticles with controllable size and their applications for Pickering emulsions, ACS Sustain. Chem. Eng. 9 (15) (2021) 5470–5480, https://doi.org/10.1021/acssuschemeng.1c01021.
[14] H. Wang, F. Xiong, Y. Tan, J. Yang, Y. Qing, F. Chu, Y. Wu, Preparation and formation mechanism of covalent–noncovalent forces stabilizing lignin nanospheres and their application in superhydrophobic and carbon materials, ACS Sustain. Chem. Eng. 9 (10) (2021) 3811–3820, https://doi.org/10.1021/acssuschemeng.0c08780.
[15] Y. Ai, H. Wang, P. Liu, H. Yu, M. Sun, R. Zhang, J. Tang, Y. Wang, S. Feng, L. Peng, Insights into contrastive cellulose nanofibrils assembly and nanocrystals catalysis from dual regulations of plant cell walls, Sci. Bull. 69 (24) (2024) 3815–3819. https://www.sciencedirect.com/science/article/pii/S2095927324004092.
[16] X. Shi, Z. Wang, S. Liu, Q. Xia, Y. Liu, W. Chen, H. Yu, K. Zhang, Scalable production of carboxylated cellulose nanofibres using a green and recyclable solvent, Nat. Sustain. 7 (3) (2024) 315–325, https://doi.org/10.1038/s41893-024-01267-0.
[17] R. Zhang, Z. Hu, H. Peng, P. Liu, Y.M. Wang, J.Y. Li, J. Lu, Y.T. Wang, T. Xia, L. C. Peng, High density cellulose nanofibril assembly leads to upgraded enzymatic and chemical catalysis of fermentable sugars, cellulose nanocrystals and cellulase production by precisely engineering cellulose synthase complexes, Green Chem. 25 (2023) 1096–1106, https://doi.org/10.1039/D2GC03744K.
[18] R. Zhang, Z. Hu, Y.T. Wang, H.Z. Hu, F.C. Li, M. Li, A. Ragauskas, T. Xia, H.Y. Han, J.F. Tang, H.Z. Yu, B.Q. Xu, L.C. Peng, Single-molecular insights into the breakpoint of cellulose nanofibers assembly during saccharification, Nat. Commun. 14 (1) (2023) 1100, https://doi.org/10.1038/s41467-023-36856-8.
[19] H. He, R. Zhang, P. Zhang, P. Wang, N. Chen, B. Qian, L. Zhang, J. Yu, B. Dai, Functional carbon from nature: biomass-derived carbon materials and the recent progress of their applications, Adv. Sci. (Weinh.) 10 (16) (2023) e2205557. https://www.ncbi.nlm.nih.gov/pubmed/36988448.
[20] B. Jiang, H. Jiao, X. Guo, G. Chen, J. Guo, W. Wu, Y. Jin, G. Cao, Z. Liang, Lignin-based materials for additive manufacturing: chemistry, processing, structures, properties, and applications, Adv. Sci. (Weinh.) 10 (9) (2023) e2206055. https://www.ncbi.nlm.nih.gov/pubmed/36658694.
[21] Q. Li, M.T. Naik, H.S. Lin, C. Hu, W.K. Serem, L. Liu, P. Karki, F.J. Zhou, J.S. Yuan, Tuning hydroxyl groups for quality carbon fiber of lignin, Carbon 139 (2018) 500–511, https://doi.org/10.1016/j.carbon.2018.07.015.
[22] R. Zhang, H.R. Gao, Y.T. Wang, B.Y. He, J. Lu, W.B. Zhu, L.C. Peng, Y.T. Wang, Challenges and perspectives of green-like lignocellulose pretreatments selectable for low-cost biofuels and high-value bioproduction, Bioresour. Technol. 369 (2022) 128315, https://doi.org/10.1016/j.biortech.2022.128315.
[23] G.Z. Zhao, Y.J. Li, G. Zhu, J.Y. Shi, T. Lu, L.K. Pan, Biomass-based N, P, and S self-doped porous carbon for high-performance supercapacitors, ACS Sustain. Chem. Eng. 7 (2019) 12052–12060, https://doi.org/10.1021/acssuschemeng.9b00725.
[24] C. Shi, L. Hu, K. Guo, H. Li, T. Zhai, Highly porous carbon with graphene nanoplatelet microstructure derived from biomass waste for high-performance supercapacitors in universal electrolyte, Adv. Sustain. Syst. 1 (1–2) (2017) 1600011, https://doi.org/10.1002/adsu.201600011.
[25] D.W. Wang, J.W. Nai, L. Xu, T. Sun, A potassium formate activation strategy for the synthesis of ultrathin graphene-like porous carbon nanosheets for advanced supercapacitor applications, ACS Sustain. Chem. Eng. 7 (23) (2019) 18901–18911, https://doi.org/10.1021/acssuschemeng.9b04209.
[26] G. Wen, Q. Gu, Y. Liu, R. Schlogl, C. Wang, Z. Tian, D.S. Su, Biomass-derived graphene-like carbon: efficient metal-free carbocatalysts for epoxidation, Angew. Chem. Int. Edit. 57 (51) (2018) 16898–16902, https://doi.org/10.1002/anie.201809970.
[27] S. Zhang, S.F. Jiang, B.C. Huang, X.C. Shen, W.J. Chen, T.P. Zhou, H.Y. Cheng, B. H. Cheng, C.Z. Wu, W.W. Li, H. Jiang, H.Q. Yu, Sustainable production of value-added carbon nanomaterials from biomass pyrolysis, Nat. Sustain. 3 (9) (2020) 753–760, https://doi.org/10.1038/s41893-020-0538-1.
[28] M. Chen, L. Guo, M. Ramakrishnan, Z.G. Fei, K.K. Vinod, Y.L. Ding, C. Jiao, Z. P. Gao, R.F. Zha, C.Y. Wang, Z.M. Gao, F. Yu, G.D. Ren, Q. Wei, Rapid growth of Moso bamboo (*Phyllostachys edulis*): cellular roadmaps, transcriptome dynamics, and environmental factors, Plant Cell 34 (10) (2022) 3577–3610, https://doi.org/10.1093/plcell/koac193.
[29] Z. Li, C. Chen, R. Mi, W. Gan, J. Dai, M. Jiao, H. Xie, Y. Yao, S. Xiao, L. Hu, A strong, tough, and scalable structural material from fast-growing bamboo, Adv. Mater. 32 (10) (2020) 1906308, https://doi.org/10.1002/adma.201906308.
[30] H.R. Gao, Y.T. Wang, Q.M. Yang, H. Peng, Y.Q. Li, D. Zhan, H.T. Wei, H.W. Lu, M. M.A. Bakr, M.M. Ei-Sheekh, Z. Qi, L.C. Peng, X.C. Lin, Combined steam explosion and optimized green-liquor pretreatments are effective for complete saccharification to maximize bioethanol production by reducing lignocellulose recalcitrance in one-year-old bamboo, Renew. Energy 175 (2021) 1069–1079, https://doi.org/10.1016/j.renene.2021.05.016.
[31] A. Alam, Y.M. Wang, F. Liu, H. Kang, S.W. Tang, Y.T. Wang, Q.M. Cai, H.L. Wang, H. Peng, Q. Li, Y.J. Zeng, Y.Y. Tu, T. Xia, L.C. Peng, Modeling of optimal green liquor pretreatment for enhanced biomass saccharification and delignification by distinct alteration of wall polymer features and biomass porosity in *Miscanthus*, Renew. Energy 159 (2020) 1128–1138, https://doi.org/10.1016/j.renene.2020.06.013.
[32] H. Peng, W.Y. Zhao, J.Y. Liu, P. Liu, H.Z. Yu, J. Deng, Q.M. Yang, R. Zhang, Z. Hu, S.L. Liu, D. Sun, L.C. Peng, Y.T. Wang, Distinct cellulose nanofibrils generated for improved Pickering emulsions and lignocellulose-degradation enzyme secretion coupled with high bioethanol production in natural rice mutants, Green Chem. 24 (7) (2022) 2975–2987, https://doi.org/10.1039/D1GC04447H.
[33] M. Si, J. Zhang, Y. He, Z. Yang, X. Yan, M. Liu, S. Zhuo, S. Wang, X. Min, C. Gao, L. Chai, Y. Shi, Synchronous and rapid preparation of lignin nanoparticles and carbon quantum dots from natural lignocellulose, Green Chem. 20 (15) (2018) 3414–3419, https://doi.org/10.1039/C8GC00744F.
[34] J. Jia, B. Yu, L. Wu, H. Wang, Z. Wu, M. Li, P. Huang, S. Feng, P. Chen, Y. Zheng, L. Peng, Biomass enzymatic saccharification is determined by the non-KOH-extractable wall polymer features that predominately affect cellulose crystallinity

in corn, PLoS One 9 (9) (2014) e108449, https://doi.org/10.1371/journal.pone.0108449.
[35] Z. Li, C. Zhao, Y. Zha, C. Wan, S. Si, F. Liu, R. Zhang, F. Li, B. Yu, Z. Yi, N. Xu, L. Peng, Q. Li, The minor wall-networks between monolignols and interlinked-phenolics predominantly affect biomass enzymatic digestibility in *Miscanthus*, PLoS One 9 (8) (2014) e105115, https://doi.org/10.1371/journal.pone.0105115.
[36] Y. Li, P. Liu, J.F. Huang, R. Zhang, Z. Hu, S.Q. Feng, Y.T. Wang, L.Q. Wang, T. Xia, L.C. Peng, Mild chemical pretreatments are sufficient for bioethanol production in transgenic rice straws overproducing glucosidase, Green Chem. 20 (9) (2018) 2047–2056, https://doi.org/10.1039/C8GC00694F.
[37] M. Hu, H. Yu, Y. Li, A. Li, Q. Cai, P. Liu, Y. Tu, Y. Wang, R. Hu, B. Hao, L. Peng, T. Xia, Distinct polymer extraction and cellulose DP reduction for complete cellulose hydrolysis under mild chemical pretreatments in sugarcane, Carbohydr. Polym. 202 (2018) 434–443, https://doi.org/10.1016/j.carbpol.2018.08.039.
[38] A. Alam, R. Zhang, P. Liu, J.F. Huang, Y.T. Wang, Z. Hu, M. Madadi, D. Sun, R. F. Hu, A.J. Ragauskas, Y.Y. Tu, L.C. Peng, A finalized determinant for complete lignocellulose enzymatic saccharification potential to maximize bioethanol production in bioenergy *Miscanthus*, Biotechnol. Biofuels 12 (2019) 99, https://doi.org/10.1186/s13068-019-1437-4.
[39] T. Pettersson, J. Hellwig, P.-J. Gustafsson, S. Stenström, Measurement of the flexibility of wet cellulose fibres using atomic force microscopy, Cellulose 24 (10) (2017) 4139–4149, https://doi.org/10.1007/s10570-017-1407-6.
[40] P. Liu, B. Pang, S. Dechert, X.C. Zhang, L.B. Andreas, S. Fischer, F. Meyer, K. Zhang, Structure selectivity of alkaline periodate oxidation on lignocellulose for facile isolation of cellulose nanocrystals, Angew. Chem. Int. Edit. 59 (8) (2020) 3218–3225, https://doi.org/10.1002/anie.201912053.
[41] T. Yang, H.J. Qi, P.W. Liu, K. Zhang, Selective isolation methods for cellulose and chitin nanocrystals, ChemPlusChem 85 (5) (2020) 1081–1088, https://doi.org/10.1002/cplu.202000250.
[42] P. Wang, G. Zhang, M. Li, Y. Yin, J. Li, G. Li, W. Wang, W. Peng, F. Cao, Y. Guo, Porous carbon for high-energy density symmetrical supercapacitor and lithium-ion hybrid electrochemical capacitors, Chem. Eng. J. 375 (2019) 122020, https://doi.org/10.1016/j.cej.2019.122020.
[43] P. Wang, G. Zhang, X.Y. Wei, R. Liu, J.J. Gu, F.F. Cao, Bioselective synthesis of a porous carbon collector for high-performance sodium-metal anodes, J. Am. Chem. Soc. 143 (9) (2021) 3280–3283. https://www.ncbi.nlm.nih.gov/pubmed/33645987.
[44] K.O. Oyedotun, F. Barzegar, A.A. Mirghni, A.A. Khaleed, T.M. Masikhwa, N. Manyala, Examination of high-porosity activated carbon obtained from dehydration of white sugar for electrochemical capacitor applications, ACS Sustain. Chem. Eng. 7 (1) (2018) 537–546, https://doi.org/10.1021/acssuschemeng.8b04080.
[45] G. Singh, R. Bahadur, A.M. Ruban, J.M. Davidraj, D. Su, A. Vinu, Synthesis of functionalized nanoporous biocarbons with high surface area for $CO_2$ capture and supercapacitor applications, Green Chem. 23 (15) (2021) 5571–5583, https://doi.org/10.1039/D1GC01376A.
[46] G. Singh, J. Lee, R. Bahadur, A. Karakoti, J. Yi, A. Vinu, Highly graphitized porous biocarbon nanosheets with tunable Micro-Meso interfaces and enhanced layer spacing for $CO_2$ capture and LIBs, Chem. Eng. J. 433 (2022) 134464, https://doi.org/10.1016/j.cej.2021.134464.
[47] L.M. Wu, S.Q. Feng, J. Deng, B. Yu, Y.M. Wang, B.Y. He, H. Peng, Q. Li, R.F. Hu, L. C. Peng, Altered carbon assimilation and cellulose accessibility to maximize bioethanol yield under low-cost biomass processing in corn brittle stalk, Green Chem. 21 (16) (2019) 4388–4399, https://doi.org/10.1039/C9GC01237K.
[48] J.T. Xu, X.Q. Chen, W.H. Shen, Z. Li, Spherical vs rod-like cellulose nanocrystals from enzymolysis: a comparative study as reinforcing agents on polyvinyl alcohol, Carbohydr. Polym. 256 (2021) 117493. https://www.ncbi.nlm.nih.gov/pubmed/33483022.
[49] A. Saleem, L. Wu, H. Shi, M. Wasim, L. Huang, W. Jia, A. Arbab, H. Tazeen, Cutting-edge innovations in lignin-based nanoparticles: a review of synthesis techniques, characterization, and diverse applications, Int. J. Biol. Macromol. 307 (Pt 2) (2025) 142123. https://www.ncbi.nlm.nih.gov/pubmed/40089243.
[50] Y. He, H. Ye, H. Li, G. Miao, Y. Hu, X. Zeng, T. You, F. Xu, Fabrication of lignin nanoparticles with adjustable size, antioxidant, antibacterial, and hydrophobic properties by a two-step fractionation, Int. J. Biol. Macromol. 297 (2025), https://doi.org/10.1016/j.ijbiomac.2025.139618.
[51] S. Zhao, S. Wang, X. Li, D. Zhang, J. Shi, W. Xu, Lignin nanoparticles: preparation strategies, surface engineering, and emerging applications-a review, Int. J. Biol. Macromol. 371 (2026) 153012. https://www.ncbi.nlm.nih.gov/pubmed/42276485.
[52] D. Tian, J.G. Hu, R.P. Chandra, J.N. Saddler, C.H. Lu, Valorizing recalcitrant cellulolytic enzyme lignin via lignin nanoparticles fabrication in an integrated biorefinery, ACS Sustain. Chem. Eng. 5 (3) (2017) 2702–2710, https://doi.org/10.1021/acssuschemeng.6b03043.
[53] M. Fernández-Martínez, J. Sardans, F. Chevallier, P. Ciais, M. Obersteiner, S. Vicca, J.G. Canadell, A. Bastos, P. Friedlingstein, S. Sitch, S.L. Piao, I.A. Janssens, J. Peñuelas, Global trends in carbon sinks and their relationships with $CO_2$ and temperature, Nat. Clim. Chang. 9 (1) (2018) 73–79, https://doi.org/10.1038/s41558-018-0367-7.
[54] C. Chen, Z. Li, R. Mi, J. Dai, H. Xie, Y. Pei, J. Li, H. Qiao, H. Tang, B. Yang, L. Hu, Rapid processing of whole bamboo with exposed, aligned nanofibrils toward a high-performance structural material, ACS Nano 14 (5) (2020) 5194–5202. https://www.ncbi.nlm.nih.gov/pubmed/32275131.
[55] B. Zhang, B.K. Biswal, J. Zhang, R. Balasubramanian, Hydrothermal treatment of biomass feedstocks for sustainable production of chemicals, fuels, and materials: progress and perspectives, Chem. Rev. 123 (2023) 7193–7294. https://www.ncbi.nlm.nih.gov/pubmed/37159561.
[56] R. Li, Y. Zheng, X. Zhao, Q. Yong, X. Meng, A. Ragauskas, C. Huang, Recent advances in biomass pretreatment using biphasic solvent systems, Green Chem. 25 (7) (2023) 2505–2523, https://doi.org/10.1039/D3GC00271C.
[57] B. Gao, J. Yu, L. Luo, L. Zhu, Z. Tang, Y. Wang, J. Kang, D. Sun, H. Peng, Y. Wang, L. Peng, H. Yu, Cascading valorization of *Miscanthus* biomass for bioethanol, lactic acid and nanomaterials via green-like pretreatment with reusable fertilizers, Renew. Energy 264 (2026), https://doi.org/10.1016/j.renene.2026.125555.
[58] H. Peng, P. Liu, J. Liu, J. Yu, B. He, Y. Yang, H. Yu, H. Kang, M. Zhou, W. Zhu, M. N. Aftab, Y. Wang, C. Fu, L. Peng, Cascading integration of genetically reduced cellulose nanofibers and ultrasound-dissected fungi mycelium for the synergistic enhancement of cellulases and saccharification with high-value bioproducts, Green Chem. 28 (12) (2026) 5347–5361, https://doi.org/10.1039/d5gc06304c.
[59] J. Wang, J. Fu, Z. Zhao, L. Bing, F. Xi, F. Wang, J. Dong, S. Wang, G. Lin, Y. Yin, Q. Hu, Benefit analysis of multi-approach biomass energy utilization toward carbon neutrality, Innovation 4 (3) (2023) 100423, https://doi.org/10.1016/j.xinn.2023.100423.
[60] A. Aui, Y. Wang, M. Mba-Wright, Evaluating the economic feasibility of cellulosic ethanol: a meta-analysis of techno-economic analysis studies, Sust. Energy Rev. 145 (2021) 111098. https://www.sciencedirect.com/science/article/pii/S1364032121003865.